Ultrafast carrier dynamics in core and core/shell CdSe quantum rods: Role of the surface and interface defects

Arianna Cretí,[1,*] Marco Anni,[2] Margherita Zavelani Rossi,[1] Guglielmo Lanzani,[1] Gabriella Leo,[3] Fabio Della Sala,[4] Liberato Manna,[4] and Mauro Lomascolo[5]

[1]*ULTRAS-INFM National Laboratory for Ultrafast and Ultraintense Optical Science, Dipartimento di Fisica, Politecnico di Milano, Piazza L. Da Vinci 32, 20133 Milano, Italy*

[2]*NNL National Nanotechnology Laboratory of INFM and Dipartimento di Ingegneria dell'Innovazione, Universitá degli Studi di Lecce, Via per Arnesano, I-73100 Lecce, Italy*

[3]*ISMN-CNR, Institute for the Study of Nanostructured Materials, Via Salaria km 29,300 00016 Monterotondo Stazione Roma, Italy*

[4]*NNL National Nanotechnology Laboratory of INFM, Università degli Studi di Lecce, Via per Arnesano, I-73100 Lecce, Italy*

[5]*IMM-CNR, Istituto per la Microelettronica e Microsistemi, Campus Universitario, Strada Prov. per Monteroni, I-73100 Lecce, Italy*

(Received 4 August 2004; revised manuscript received 10 June 2005; published 30 September 2005)

Femtosecond pump-probe spectroscopy, in the visible spectral range, is used to study fast processes after photoexcitation in quantum confined wurtzite CdSe core and CdSe/CdS/ZnS core/shell nanorods. Effective-mass theory is applied to assign the energy levels in linear absorption spectra. Sequential bleaching of the excitonic states and photoinduced absorption are observed in the transmission difference spectra. A strong difference was found between the core and core/shell samples. In fact, in the transient transmission difference spectra, the decay time of the higher energy states is faster in the core than in the core/shell samples (200 fs versus 500 fs), due to the trapping in the unpassivated surface states of the bare core. Stimulated emission (SE) has been achieved in CdSe core and core/shell quantum rods at room temperature. As a striking feature, the SE is sustained for a shorter time in the core/shell sample (25 ps) compared with the core sample (50 ps). We demonstrate that this result is due to the competition between SE and photoinduced absorption from defect states in the midgap of the core/shell sample. Such midgap states are related to the formation of extended defects at the core/shell interface, due to lattice strain relaxation.

DOI: 10.1103/PhysRevB.72.125346 PACS number(s): 78.47.+p, 78.67.Bf, 73.22.−f, 71.55.−i

I. INTRODUCTION

Many advances in the synthesis of colloidal semiconductor nanocrystals have been achieved in the last few years, allowing for size and shape control.[1–3] Of particular interest for scientific and technological applications[4,5] are the rod-shaped nanocrystals that display one-dimensional quantum properties.[1] Quantum confined CdSe rods (QRs) are currently largely investigated due to the ability to tune their emission wavelength in the visible spectral range through the control of the rod diameter. In addition, due to their dimensional anisotropy, polarized emission has also been detected for such nanorods.[6]

In recent studies, lasing from CdSe QRs inserted in microcavity and optical gain from CdSe in hexane solution at ambient temperature have also been achieved.[7–9] Moreover, Htoon *et al.*[9,10] have demonstrated beneficial features for lasing applications in quantum rods, compared to quantum dots, such as a reduced lasing threshold due to enhanced absorption cross section, and increased lifetimes of optical gain, due to suppressed Auger decay and photoinduced absorption (PA) losses.

The interesting properties of QRs as laser materials have driven the research for improvements in their emission quantum yield and photostability. Enhancement by over one order of magnitude in the CdSe rod photoluminescence (PL) quantum yield (QY) and stabilization against surface oxidization have been obtained by epitaxial overgrowth of an inorganic shell of a higher band gap material.[11,12] As already observed in core-shell QDs,[13–16] the PL QY in rods tends to increase by increasing the shell thickness up to a critical thickness, which depends on both the core size and the lattice mismatch between core and shell materials.[11,12] A further increase in the shell thickness causes a noteworthy decrease in the QY. This behavior has been ascribed, in both dots and rods, to the generation of defects at the core/shell interface due to the lattice strain relaxation.[13,14] Up to now, few high resolution transmission electron microscopy (TEM) observations give a clear evidence of misfit dislocation in these systems.[17]

Despite the strong improvement in the PL properties of the core/shell quantum rods compared with bare core rods, no studies have yet been reported on the ultrafast carriers relaxation dependence on the interface of core/shell nanorods.

In this work we have investigated the ultrafast carrier dynamics, in bare CdSe core and core/shell CdSe/CdS/ZnS quantum rods, by means of femtosecond pump and probe transient spectroscopy in the visible spectral range, in order to have a deeper insight into the competition between stimulated emission (SE), which is necessary to have optical gain, and photoinduced absorption, and to clarify how the shell modifies these processes.

Our results show that the nonlinear optical response in QRs is dominated by state filling leading to pronounced bleaching band at the energies of the allowed optical transitions. The electron-hole transitions giving rise to the different bleaching resonances are determined by comparison with the states theoretically calculated by an effective-mass theory for

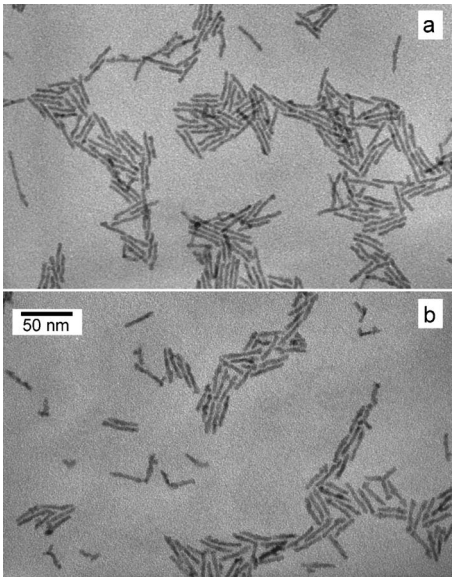

FIG. 1. Transmission electron microscopy (TEM) images of the (a) CdSe core and (b) CdSe/CdS/ZnS QRs.

core and core/shell samples. The bleaching recovery is multiexponential, indicating that different photoinduced processes are involved in the system relaxation. We observed faster bleaching recovery in the core sample, suggesting an efficient trapping mechanism by surface states (passivated in core/shell sample) which involves mainly the population of the higher energy states. Moreover SE is observed in the emission spectral range of both samples but, surprisingly, despite the tenfold improvement of the PL QY due to the shell overgrowth, the core/shell sample exhibits a smaller SE and a faster SE decay time. We show that these results are due to spectral overlap between SE and photoinduced absorption, which is attributed to extended midgap defect states, due to partial strain relaxation at the core-shell interface.

II. METHODS

A. Experiment

Core CdSe and core/shell CdSe/CdS/ZnS nanorods were prepared following the procedure described in Ref. 11. TEM measurements were performed on a FEI Tecnai 12 operating at 120 kV (UC Berkeley Electron Microscope Laboratory, UC Berkeley, USA). The images of the CdSe core and core/shell QRs are shown in Fig. 1.

The average diameter and length size of the CdSe core, obtained by the analysis of the TEM micrographs, is 3.6 $\times 29$ nm (with a size dispersion of 14% and 17%, for diameter and length, respectively). The shell thickness was determined by the difference between the diameter of the core and the core/shell nanorods. From the measurements of more than 100 nanorods, an average shell thickness of about 0.80 ML was estimated (1 ML=d_{111} lattice spacing of the shell material and d_{111}=3.1 Å for ZnS). Continuous wave optical spectroscopy (absorption, photoluminescence, and photoluminescence excitation) spectra were recorded on a Variant-Cary UV-Vis 500 spectrophotometer and on a Variant-Cary Eclipse fluorescence spectrometer, respectively. Room temperature photoluminescence quantum yield of the nanocrystals in chloroform solution was determined by comparing the integrated emission with that of rodamine 6G dye in ethanol solution with equal optical density at the excitation energy (2.54 eV). The QY values were corrected for the differences in refractive index between chloroform and ethanol. The experimental setup for time resolved pump-probe spectroscopy is based on an amplified Ti-sapphire laser which provides 150 fs, 750 μJ pulses at 780 nm, at 1 KHz repetition rate. The pump beam is obtained by second harmonic generation (390 nm, 3.18 eV) in 1-mm thick lithium triborate crystal and it is linearly polarized at the magic angle (54,7°) with respect to the probe. The large spectrum probe beam is obtained by white supercontinuum generation in a 2-mm thick plate of sapphire and it is collected and focused onto the sample only by mirrors to minimize frequency chirp effect. Differential transmission spectra at a given pump-probe delay were recorded by an optical multichannel analyzer averaging on a large number of laser pulses. Differential transmission dynamics were obtained using a standard lock-in technique and 10 nm band width interference filters to select the probe wavelength. All the experiments discussed in this paper were performed with nanorods dispersed in chloroform solution and at room temperature.

B. Theory

The hole-electron transitions, giving rise to the absorption resonances, have been determined by solving numerically the three-dimensional single-particle effective-mass Schrödinger equation, using discretization[18] with a step of 0.2 nm. The lowest (highest) electron (hole) eigenvalues are computed using a modified Davidson algorithm.[19,20] The used values for the electron and hole effective mass were 0.13 (Ref. 21) and 0.40, respectively. The latter value accurately reproduced the evolution with the radius of the first valence level as reported in Ref. 22. We used an infinite hole barrier and an electron barrier of 8.9 eV.[23,24] The value used for the energy gap of wurtzite CdSe at 300 K was 1.74 eV.[25]

The excitation energies are calculated by considering single-particle electron-hole transitions with an exciton correction due to the electron-hole Coulomb attraction (a dielectric constant of 9.3 is used).

The electron-hole Coulomb attraction is computed as $\langle \psi_h | V_e | \psi_h \rangle$, where ψ_h is the hole wave function and V_e is the electrostatic potential of the electron wave function which is obtained solving a three-dimensional Poisson equation. For the rods investigated here, the calculated exciton correction was around 30–40 meV.

The final optical spectra are obtained by a Gaussian convolution with rms=0.05 eV, which reproduces the experimental broadening.

III. RESULTS

A. Linear absorption and differential transmission spectra

The linear absorption spectra are depicted in Figs. 2(a) and 2(b), for CdSe core QRs and CdSe/CdS/ZnS graded

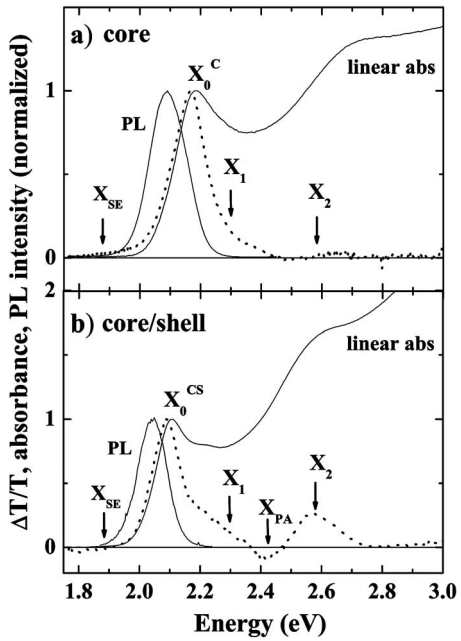

FIG. 2. Linear absorption spectra (abs) and $\Delta T/T$ differential transmission spectra (dotted lines) recorded 4 ps after excitation at 3.18 eV with 200 fs–160 μJ/cm^2, of (a) CdSe and (b) CdSe/CdS/ZnS QRs. Photoluminescence (PL) spectra obtained after excitation at 3.18 eV are also shown for both samples. All spectra are normalized for comparison.

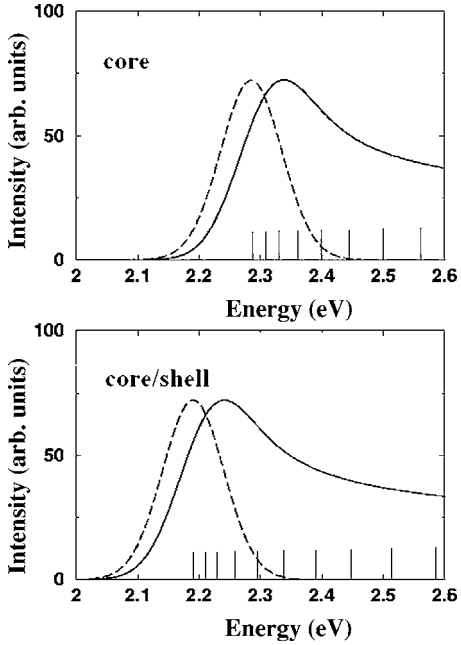

FIG. 3. Calculated absorption (solid-line) and PL (dashed-line) spectra of CdSe core and core/shell QRs.

core/shell QRs, respectively. Both samples present a structured linear absorption spectrum with defined features. The absorption spectra show a first absorption maximum at 2.19 eV for CdSe core and at 2.11 eV for the core/shell sample. The redshift of the first absorption peak in the core/shell sample is an indication that a shell has been grown on the cores. Figure 2 shows also the PL spectra of core and core/shell QRs. In the samples, the PL maximum is Stokes shifted from the first absorption peak by 100 and 70 meV, respectively. The PL signal provides an additional confirmation of the presence of the shell as in the core/shell samples the luminescence quantum yield increases tenfold, going from 0.3% in the core sample to 3% in the core/shell sample.[11–16]

The normalized chirp-free differential transmission ($\Delta T/T$) spectra of core and core/shell QRs for a pump and probe delay of 4 ps are reported in Fig. 2 (dotted line). In these measurements an excitation fluence of 160 μJ/cm^2 has been used, corresponding to initial QRs population of few *e-h* pair per QRs on average.

Three absorption bleaching peaks can be identified for both core and core/shell samples: $X_0^{C(CS)}$, X_1, X_2, centered at 2.17 (2.09) eV, 2.29 eV, and 2.58 eV, respectively. The first peak is redshifted of ~20 meV for both samples, compared to the linear absorption maximum. The X_1 and X_2 bands are less intense in core QRs, suggesting a higher photoinduced absorption competing with bleaching. Moreover, in core QRs a region of positive $\Delta T/T$ is visible at energy lower than 2.0 eV while no clear evidence of positive $\Delta T/T$ is present in core/shell QRs below the absorption onset. Finally, the $\Delta T/T$ spectrum of the core/shell sample shows a photoinduced absorption band centered at 2.42 eV.

B. Theory

The calculated absorption and PL spectra for the core and the core/shell rods are shown in Fig. 3. The presence of the shell reduces the lowest excitation energy by about 0.1 eV. The shape of the absorption spectra is the result of the convolution of several energy transitions (shown as narrow lines in Fig. 3) and as a consequence its peak does not correspond to the lowest energy transition, from which the PL originates. All the reported transitions have S character, due to the length of the rod.

C. Time-resolved differential transmission spectra: Bleaching and stimulated emission

Time-resolved differential transmission $\Delta T/T$ measurements were performed at several probe energies in order to study the excitation and relaxation dynamics of the different excited states of the core and core/shell sample. As a general trend, all the kinetics follow a multiexponential decay.

1. CORE sample

We first studied the excited states associated with the bleaching signal, pumping with 160 μJ/cm^2 and probing the X_0^C, X_1, and X_2 peaks. Figure 4 shows the data obtained. All

TABLE I. Time constants for core sample. All the constants are expressed in picoseconds.

	τ_{rise}	τ_{d1}	τ_{d2}	τ_{d3}	τ_{d4}
X_0	0.480±0.020	1.5±0.1	15±5	128±2	1300±100
X_1	0.345±0.025	0.7±0.1	20±5	130±10	1250±100
X_2	0.210±0.030	0.220±0.010	22±5	140±10	1300±100

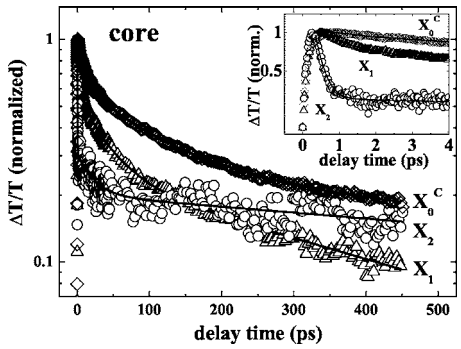

FIG. 4. Bleaching kinetics recorded at X_0^C=2.17 eV, X_1 =2.29 eV, and X_2=2.58 eV for the core sample, at an excitation fluence of 160 μJ/cm^2, together with multiexponential best fits. Inset: zoom in the first 4 ps.

the traces present a nonexponential decay that have been fitted with a multiexponential decay with four time constants (Fig. 4, continuous lines). The best fit values of the decay and the rise times, defined as time interval from the 10% to the 90% of the rising signal, are reported in Table I. The main results are the following:

(i) The rise time and the fastest decay time τ_{d1} continuously increase as the energy level decreases.

(ii) The longer decay times τ_{d2}, τ_{d3}, and τ_{d4} are almost identical for the three bands.

In order to investigate the role of the nonlinear relaxation processes, such as Auger recombination and/or exciton-exciton scattering on the system relaxation, we performed differential transmission measurements for different excitation fluences on the X_0^C and X_2 bands.

Figure 5 shows the bleaching dynamics of the lowest exciton transition X_0^C at different excitation fluences, corresponding to different values of the average numbers N_0 of *e-h* pairs excited per QRs. The average numbers N_0 are obtained as $N_0=j_p\sigma_0$ where j_p is the excitation fluence and σ_0 is the absorption cross section of the rod at a pump spectral energy.[9] The signal rise time and the different decay times show different dependence on the excitation fluence in particular:

(i) As the excitation fluence increases from 16 μJ/cm^2 (N_0=0.3) to 160 μJ/cm^2 (N_0=3.5) the signal rise time and the fastest decay time τ_{d1} increase from 0.280 to 0.480 ps and from 0.80 to 1.5 ps, respectively.

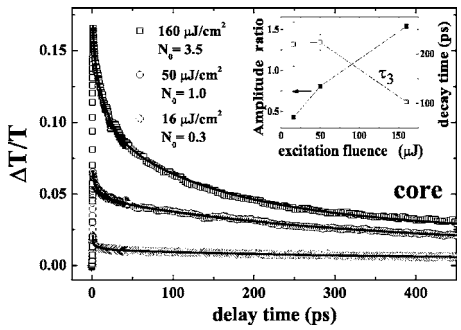

FIG. 5. Bleaching kinetics recorded at X_0 band in the core sample for different pump fluences.

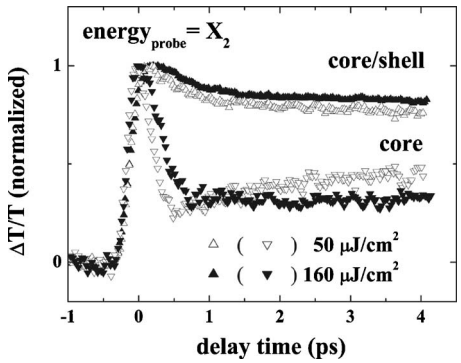

FIG. 6. Bleaching kinetics recorded at 2.58 eV (X_2 band) in the core and core/shell samples for different pump fluences.

(ii) The decay time τ_{d2} and the longest decay time τ_{d4} have the same value within the statistic error for all excitation fluences.

(iii) The decay time τ_{d3} decreases with the pump fluence and the contribution to the decay increases. This is evidenced in the inset of Fig. 5 where we have plotted the best fit τ_{d3} values (open squares) and the amplitude (solid squares) of the τ_{d3} component, relative to the slow component, as a function of the excitation fluence.

The relaxation dynamics of the X_2 bleaching band, for an excitation fluence of 50 and 160 μJ/cm^2, are reported in Fig. 6. At the lowest excitation fluence a fast decay and a clear increase of the bleaching signal is visible for pump and probe delay higher than 0.7 ps, indicating that the absorption bleaching of the X_2 feature is spectrally overlapped to some photoinduced absorption signal that initially overcomes. As the excitation density increases the fast relaxation becomes slower and the photoinduced absorption is less evident.

Finally, we studied the relaxation dynamics in the emission range of the sample. Figure 7 shows the kinetic recorded at a probe energy of 1.88 eV, at an excitation fluence of 160 μJ/cm^2. As evident from the inset, a photoinduced absorption signal dominates in the first few hundreds of femtoseconds, while positive $\Delta T/T$, possibly due to SE, is visible for larger delays. The positive signal rise time is about 600 fs, while the decay is biexponential, with a fast decay time τ_{S1} of about 14 ps and a longer decay time τ_{S2} of about 1250 ps. The positive signal formation time is longer than

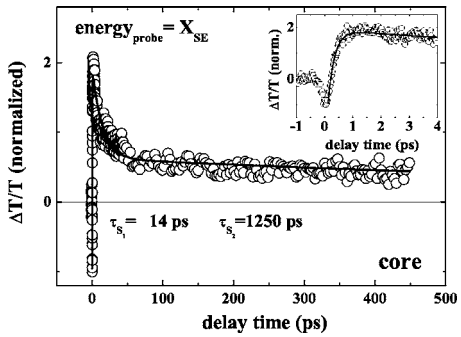

FIG. 7. $\Delta T/T$ dynamic recorded at 1.88 eV for the core sample, at an excitation fluence of 160 μJ/cm^2, and best fit. Inset: zoom in the first 4 ps.

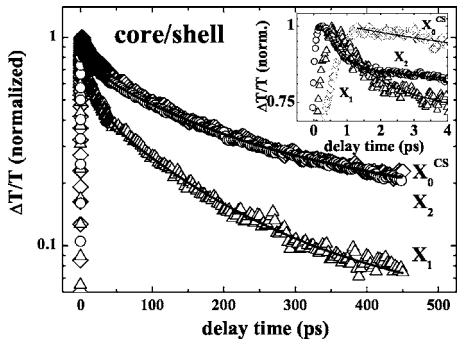

FIG. 8. Bleaching kinetics recorded at X_0^{CS}=2.10 eV, X_1 =2.29 eV, and X_2=2.58 eV for the core/shell sample, at an excitation fluence of 160 μJ/cm^2, together with multiexponential best fits. Inset: zoom in the first 4 ps.

the rise time of all the bleaching bands, while the two decay times are very close to the bleaching decay time constants τ_{d2} and τ_{d4}. The same trend has been observed for a probe energy of 2.00 eV not shown.

2. Core/shell sample

The role of the shell is considered in this section. Figure 8 shows the $\Delta T/T$ dynamics of the excited states X_0^{CS}, X_1 and X_2 associated with bleaching peaks, obtained for 160 μJ/cm^2 excitation fluence. All data have been fitted with a multiexponential decay, with four time constants. The best fit decay and rise time (defined as time interval from the 10% to the 90% of the rising signal) are reported in Table II.

The main results are the following:

(i) The rise time of the bleaching signal increases as the excited state energy decreases, from about 280 fs of X_2 to about 1 ps of X_0^{CS}.

(ii) The fastest decay time τ_{d1} of the X_2 and X_1 feature coincides, within the fitting error, with the rise time of the nearest lower level, X_1 and X_0^{CS}, respectively.

(iii) The three longer decay times τ_{d2}, τ_{d3}, and τ_{d4} have the same value (within the statistic error) for all states.

In addition, we notice that all rise times and all fastest decay times τ_{d1} are longer than the corresponding ones of the core QRs.

Also in the core/shell sample, the role of nonlinear relaxation processes has been studied by measuring the excitation fluence dependence of the X_0^{CS} and X_2 bleaching band. The excitation fluence dependence of the X_0^{CS} bleaching relaxation is reported in Fig. 9. As the excitation fluence increases from 50 to 160 μJ/cm^2 both the rise time and the first decay time constant increase from 0.280 to 0.99 ps and from 0.60 to 9 ps, respectively. The decay times τ_{d4} and τ_{d2} are instead independent of the pump fluence, while τ_{d3} decreases from about 200 ps at 50 μJ/cm^2 to about 120 ps at 160 μJ/cm^2.

TABLE II. Time constants for core/shell sample. All the constants are expressed in picoseconds.

	τ_{rise}	τ_{d1}	τ_{d2}	τ_{d3}	τ_{d4}
X_0	0.990±0.030	9±1	27±10	122±10	565±20
X_1	0.530±0.030	0.82±0.05	17±5	100±10	550±20
X_2	0.280±0.015	0.487±0.014	22±5	120±10	550±20

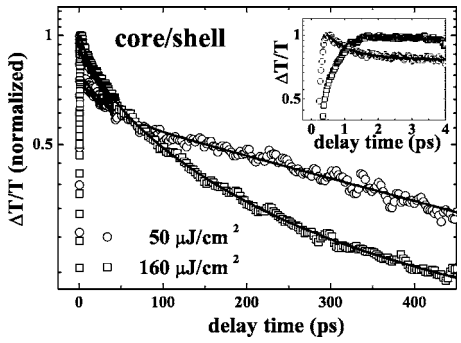

FIG. 9. Bleaching kinetics recorded at X_0 band in the core/shell sample for different pump fluences.

Figure 6 shows the comparison between the relaxation dynamics of the X_2 state in core and core/shell samples, for different pump fluences. It clearly results that the fraction of the bleaching signal recovered in the first 500 fs is larger in the core than in the core/shell sample, at the same laser excitation intensity. At 50 μJ/cm^2, 80% of the core signal recovers in 500 fs while only 15% of the bleaching signal recovers in the core/shell in the same time; at 160 μJ/cm^2, 55% of the excitation recovers in the core sample, while only 10% of the excitation recovers in the core/shell one. We can thus argue that different relaxation paths exist in the two samples.

We also recorded the $\Delta T/T$ dynamics in the low energy side spectrum, where stimulated emission is expected. This is shown in Fig. 10 where we report the trace recorded at 1.88 eV, at an excitation fluence of 160 μJ/cm^2. This $\Delta T/T$ dynamic shows a photoinduced absorption in the first picosecond, and then a positive signal. The positive signal relaxation is biexponential, with a fast decay times τ_{S1} of about 19 ps and a longer one τ_{S2} of about 150 ps. These decay times coincide with the bleaching decay time τ_{d2} and τ_{d3}. At delay time higher than about 150 ps the signal becomes negative, indicating that the PA process is stronger than the absorption bleaching and the eventual SE.

Finally photoinduced absorption processes are observed in $\Delta T/T$ traces recorded at 1.77 and 2.43 eV, at an excitation

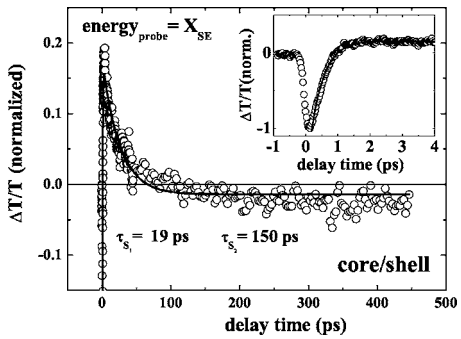

FIG. 10. $\Delta T/T$ dynamic recorded at 1.88 eV of core/shell sample, at an excitation fluence of 160 μJ/cm^2. Inset: zoom in the first 4 ps.

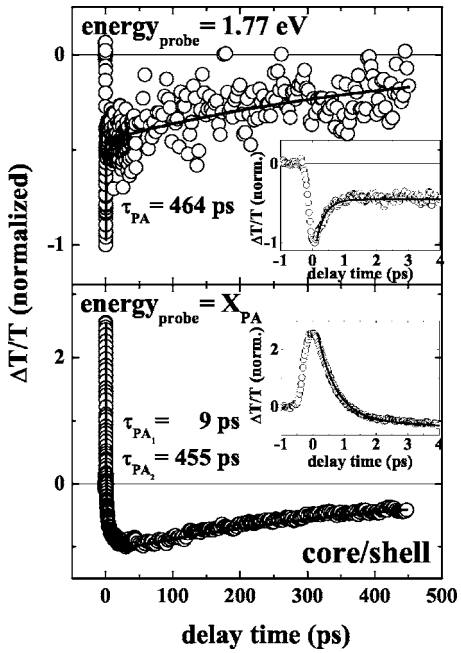

FIG. 11. Photoinduced absorption at 1.77 and at 2.43 eV of core/shell sample, at an excitation fluence of 160 $\mu J/cm^2$, and best fits. Inset: zoom in the first 4 ps.

fluence of 160 $\mu J/cm^2$ (Fig. 11). The PA dynamic at 1.77 eV shows a very fast rise time and a nonexponential decay with a fastest decay time of about 300 fs and a longest one of about 464 ps; the signal at 2.43 eV is overcome by the bleaching in the first 1 ps, then PA dominates and the decay is biexponential with decay times τ_{PA1} of about 9 ps and τ_{PA2} of about 455 ps.

IV. DISCUSSION

A. Electronic structure and differential transmission spectra

The calculated optical spectra accurately reproduce the experimental lowest absorption peak and the difference between the core and the core-shell samples. The core-shell absorption and PL are redshifted with respect the core because in the former the electron wave function can tunnel into the shell, increasing the delocalization of the electrons that lowers the confinement energy and consequently the energy of the excited state.[13–15] Moreover, the redshift of the absorption peak definitely rules out the formation of an alloy of the core and shell materials. In this case a blueshift is expected due to larger energy gap of the alloy compared with the band gap of the CdSe. The Stokes shift between the PL maximum and the first absorption peak is assigned not only to the dark-exciton effect,[26] but also to the shift between the lowest excited state (from which the PL originates) and the absorption peak, which is the result of the convolution of the S-type states close to the QRs band gap (see Fig. 3).

In the differential transmission spectra of core and core/shell QRs, the observed well-defined bleaching signals $X_0^{C(CS)}$ are attributed to the state filling mechanism.[27] In particular, the peaks observed are assigned to the convolution of the absorption bleaching of the different transitions in the lowest energy side of the absorption spectra (Fig. 3). Similarly, even the further bands observed at the higher energy side of the spectra (X_1 and X_2) are attributed to the convolution of the bleaching of higher lying states. In addition, we have observed that the $X_0^{C(CS)}$ transition in both samples is redshifted with respect to the linear absorption peak. In nanocrystals, band-edge optical nonlinearities arise primarily from state filling, leading to bleaching of optical transition and Coulomb multiparticle interactions, namely, the Stark effect, which results in transition shift. However, the Stark effects dominate at shorter delay time (<1 ps) (Refs. 27 and 28) while the observed redshift is present also for pump and probe delay higher than 4 ps, then we are unable to explain the observed redshift. The bleaching band at the lower energy side is more broadened in the core sample spectrum with respect to the core/shell sample, indicating that probably SE occurs. The positive $\Delta T/T$ signal in the emission range of both samples has been attributed to SE as it is much larger that the expected absorption bleaching. The latter can be easily estimated by remembering that, in the limit of small signals, the absorption bleaching is proportional to the sample absorption. The relationship between the measured $\Delta T/T$ signal and the optical density variation $\Delta\alpha d$ is given by

$$\Delta T/T = e^{-\Delta\alpha d} - 1 \approx -\Delta\alpha d. \tag{1}$$

For this reason, in the absence of PA and SE, the absorption bleaching and the linear absorption line shapes have to be identical. Then the absorption bleaching contribution at the emission peak energy ($\Delta T/T_{\mathrm{em}}^{\mathrm{bl}}$) can be estimated from the absorption bleaching at the X_0 energy ($\Delta T/T_{X_0}^{\mathrm{bl}}$), and the linear absorption at the corresponding energies ($\mathrm{Abs}_{\mathrm{em}}$ and Abs_{X_0}), by the relation

$$\frac{\Delta T/T_{\mathrm{em}}^{\mathrm{bl}}}{\Delta T/T_{X_0}^{\mathrm{bl}}} = \frac{\mathrm{Abs}_{\mathrm{em}}}{\mathrm{Abs}_{X_0}}. \tag{2}$$

The obtained value for the core (core/shell) sample is about 0.6% (0.2%), which is smaller that the observed signal, of about 2% (0.5%).[31]

On the contrary the bleaching bands, at the higher energy, have a very small signal in the core sample with respect to the core/shell sample.

These differences and the absence of a clear PA band, indicate that stimulated emission and PA processes at higher energy are strongly modified by the presence of the shell.

PA processes attribution is an important step for the understanding of the light amplification processes in colloidal nanoparticles. Usually the inability to achieve optical gain in CdSe quantum dots[30] and quantum rods[8] at room temperature in solution (after high-energy excitation) has been attributed to a competing induced absorption, possibly due to trapped charge carriers at the particles interface, below the absorption onset and resonant to the steady state PL spectrum. Very recently Malko *et al.*[32] have studied, in detail, the competition between optical gain and excited-state absorption in CdSe quantum dots as a function of size, surface passivation, and solvent matrix identity, and their results

have confirmed that the PA resonant to the emission is not an intrinsic mechanism, but it is due to superficial defect states. This is confirmed by the surface dependence of the PA, which is very similar in most of the solvents (like hexane, toluene, and chloroform), but it is strongly reduced in trioctylphosphine (TOP) solutions, due to the good surface passivation. We then attribute the observed PA signal, which is modified by the presence of the shell (reduced at high energy and enhanced at low energy) to PA from superficial defects states. The details of the defect states filling and depletion dynamics, and of their energy position are discussed in the next section.

B. Carrier relaxation processes

A quantitative analysis of the bleaching decay curves, recorded at $X_0^{C(CS)}$, X_1 and X_2 features, was performed using a four-exponential fit, which indicates that different relaxation processes are present. As a matter of fact, the experiments were performed on an ensemble of size-dispersed quantum rods, hence all the features are inhomogeneously broadened. The observed relaxation dynamics arises from the contribution of all the single rod dynamics, which might depend on the rod dimensions.[29] The above mentioned process may contribute to the overall multiexponential behavior.

1. Core sample

From the analysis of the data from the core samples, obtained for 160 μJ/cm^2 excitation fluence, we observe that the initially pump populated states relax to the highest X_2 band in about 210 fs. It is interesting to observe that the fastest relaxation time of X_2 ($\tau_{d1} \simeq 220$ fs) is faster than the X_1 rise ($\simeq$345 fs). This indicates that the thermalization process to X_1 band, taking place in about 345 fs (rise time of X_1), is in competition with another depletion channel of X_2, which can be attributed to carrier surface trapping. A trapped carrier fraction of about 60% can be estimated by using the simple rule: $\tau_{d1}^{-1}/[\tau_{d1}^{-1}+(\tau_{\text{rise}})^{-1})]$). Only the 40% reaches the X_1 band, then relaxes by thermalization and reaches the X_0^C band (the rise time of X_0^C is comparable to the fastest relaxation time τ_{d1} of X_1).

The system then relaxes by interband processes. Trapping in defect states is responsible for the fastest bleaching decay time (1.5 ps). This is confirmed by the measurements at low excitation fluence, because the fastest bleaching decay time decreases (from 1.5 to 0.80 ps).

Note that the trapping mechanism becomes less important as the state energy decreases (τ_{d1} bleaching decay time becomes longer). We thus conclude that the defects trapping mechanism is more probable when the excitation is on highest excited states, suggesting a higher density of defects states close to X_2 [Fig. 12(a)].

The nature of the fastest relaxation mechanism from X_2 is confirmed by differential transmission measurements for different excitation fluences. As a matter of fact, in Fig. 6 we observed that this process becomes slower by increasing the pump intensity, and so it cannot be attributed to nonlinear recombination processes such as, for instance, Auger recombination, because this mechanism would lead to the opposite

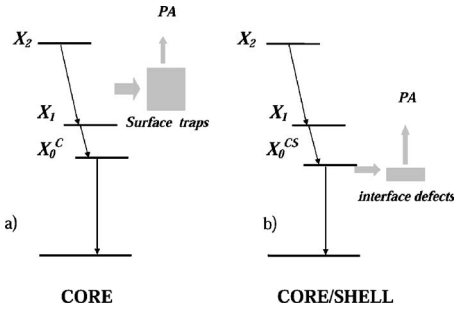

FIG. 12. (a) Energy level diagram for the core sample. (b) Energy level diagram for the core/shell sample.

behavior. This result, together with the observed reduced importance of the photoinduced absorption at the highest excitation density, strongly suggests that the rapid decay process comes from excited states depletion due to trapping, which is partially saturated at the highest excitation density. The relaxation from defects states takes place in about 130 ps (τ_{d3}), due to nonradiative processes. The nature of these nonradiative relaxation processes is clarified by the intensity dependence observed in the bleaching decay dynamics of the lowest exciton transition X_0. The decrease of τ_{d3} as the excitation fluence increases, together with the increasing importance of this process, suggest that the relaxation is due to Auger recombination. As the trapped carriers populate localized states, an Auger recombination between trapped carriers is unlikely. The observed results can be instead due to Auger relaxation of trapped carriers, due to scattering with free carriers.[33,34] This Auger process offers then a carrier recombination mechanism after initial surface trapping and, as the pump intensity increases, it becomes faster and more important. As this relaxation component is still present at the lowest pump fluence, we conclude that even under this excitation condition carrier-carrier scattering cannot be neglected.

In order to obtain another direct evidence that excitation trapping competes with the carriers relaxation to the emitting state, photoluminescence excitation (PLE) spectra have been measured. In Fig. 13(a) we show the PLE spectrum of core sample, detected at about the maximum of PL spectrum (2.09 eV), together with the absorption and PL spectra. It is evident that the PLE line shape follows the absorption one only

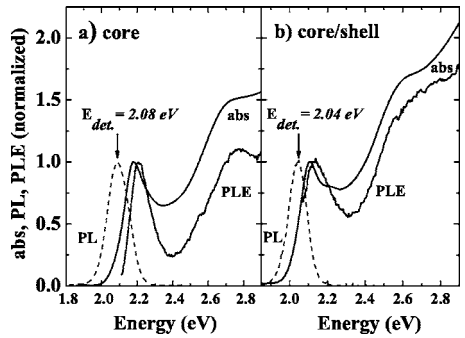

FIG. 13. (a) Absorption, PL, and PLE spectra detected at the maximum of the PL spectrum for the core sample. (b) Absorption, PL and PLE spectra detected at the maximum of the PL spectrum for the core/shell sample.

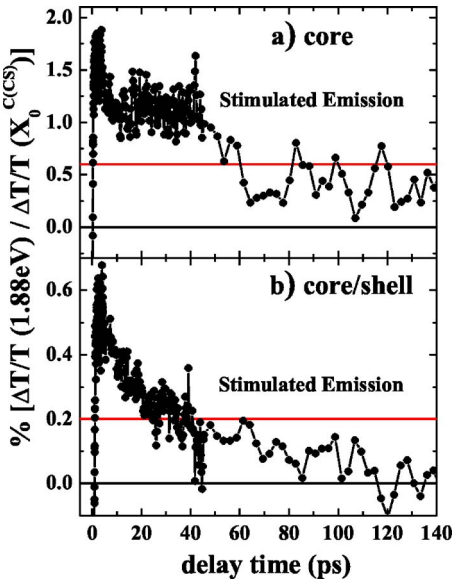

FIG. 14. (Color online) Ratio between $\Delta T/T$ dynamics (in percentage) of (a) core and (b) core/shell sample, recorded at 1.88 eV and $X_0^{C(CS)}$, respectively. The continuous line represents the SE threshold resulting from linear abs spectrum.

for the X_0 band, while for energy >2.3 eV, the PLE spectrum is always below the absorption one. This result clearly demonstrates that the carriers populating the high excited states can be efficiently trapped before relaxing to the first excited state.

Finally, we have observed that SE is achieved and sustained for a long time at low energy (1.88 eV) in the core sample. In particular, this signal relaxation is biexponential and the decay times are similar to the bleaching decay time τ_{d2} and τ_{d4}. The matching decay times for the bleaching and the positive signal at 1.88 eV suggests that the same relaxation process is involved in both signal relaxations. We then attribute τ_{d2} and τ_{d4} to the system relaxation from the emitting excited states.

In order to determine how long after the pump pulse the SE signal is stronger than the PA one we have analyzed the ratio between the transient dynamics recorded at 1.88 eV and at X_0, respectively. As long as this ratio is higher than the bleaching signal ratio, estimated from the absorption spectra, SE is larger than PA (see the Appendix). For this reason in the following the bleaching signal ratio can be considered as a net SE threshold. As reported in Fig. 14(a) this ratio results to be above the net SE threshold of 0.6% only in the first 50 ps after the pump pulse. As a stimulated emission stronger than the photoinduced absorption is a necessary condition to have gain in the sample, 50 ps can be considered as an upper limit for the gain lifetime in the core rods.

In fact as the optical gain is essentially a biexciton phenomenon, its lifetime is limited by the Auger relaxation, whose rate increases as the excitation density is increased to reach the population inversion. In our case net SE is observed in a time interval, shorter than the observed Auger decay time (130 ps), and comparable to the gain lifetime observed for this system in literature.

2. Core/shell sample

From the analysis of the core/shell data, obtained for 160 μJ/cm^2 excitation fluence, it results that in the early 280 fs the carriers distribute themselves among few energy states at high energy (around X_2 feature). In the following 500 ps the population of the higher energy states relaxes rapidly to the lower states (X_1), and finally in the 1 ps in X_0^{CS} state. The system then relaxes by interband processes. It is important to note that the faster decay times τ_{d1} are longer than the corresponding ones of core sample. This means that a carriers depletion channel has been suppressed. This conclusion is supported by the comparison of the X_2 feature relaxation dynamics in both samples, reported in Fig. 6. The effect of fast carrier trapping by surface defects, evident in core quantum rods, is not present in the core/shell sample. The absence of further relaxation pathways in addition to intrinsic intraband relaxation processes in X_2 core/shell dynamics, clearly demonstrates the passivation of these surface defects by the shell overgrowth.

We then conclude that:

(i) In the core sample the bare surface defects introduce energy states resonant to the high energy intrinsic levels.

(ii) These energy states are passivated by the shell.

(iii) The large increase of QY in the core/shell sample is due to an increase in the population of the emitting state, by eliminating electron trapping from higher excited states.

On the contrary the fastest relaxation process of X_0^{CS} (τ_{d1}) at low excitation density, is faster than the corresponding process in the core sample. This suggests that in the core/shell sample the carriers in X_0^{CS} can be trapped in new defect states, close in energy to X_0^{CS}, introduced by the shell. This conclusion is confirmed by the increase of τ_{d1} with the excitation fluence, due to defect saturation.

The reduction of the trapping from highly excited states due to the shell growth can be observed in Fig. 13(b), in which the comparison between absorption and PLE spectra, detected at 2.04 eV, is reported.

The figure shows that also for the core/shell sample the PLE spectrum follows the absorption spectrum only for the X_0 band, but at higher energy the difference between the absorption and PLE spectra is clearly reduced with respect to the core sample, indicating that the trapping of highly excited carriers is reduced by the shell overgrowth.

Moreover, the analysis of the bleaching decay dynamics of the lowest exciton transition X_0^{CS}, as a function of the excitation fluence, shows also that in the core/shell sample the Auger recombination process is responsible for the long decay time τ_{d3}.

Also in the core/shell sample SE is observed at 1.88 eV. The SE relaxation dynamics results to be biexponential with time constants $\tau_{g1}=19$ ps and $\tau_{g2}=150$ ps, which are similar to the bleaching decay times τ_{d2} and τ_{d3}. This suggests that the time constant τ_{d2} is related to relaxation from the emitting excited states, as already observed in the core sample and τ_{d3} is related to the Auger recombination process. The SE maximum lifetime in the core/shell rods (150 ps) is reduced with respect to the core sample (1250 ps). This result clearly indicates that in the core/shell sample nonradiative relaxation channels from X_0^{CS} are present, that reduce the X_0^{CS} lifetime.

Additionally, as already observed in the discussion of Fig. 2, the stimulated emission is clearly spectrally overlapped to a photoinduced absorption process, as the $\Delta T/T$ signal at 1.88 eV becomes negative for pump-probe delays higher than about 70 ps.

In order to estimate how long SE is stronger than PA, we analyzed the ratio between the transient dynamics recorded at 1.88 eV and at X_0, respectively. This is reported in Fig. 14(b). The ratio results to be above the net SE threshold of 0.2%, only in the first 25 ps. Then, in the core/shell sample the SE signal is smaller, with a faster decay relaxation, and it is higher that the spectrally overlapped PA for a shorter time. Also in the core/shell sample 25 ps can be considered an upper limit for the optical gain lifetime.

Concerning the PA attribution it is important to observe that at both the probed energies (1.77 and 2.43 eV) the PA relaxation dynamics is different from the SE one, indicating that the PA do not come from the intrinsic emitting states of the rod. Therefore we attribute those signals to PA from defects. The 2.43 eV PA shows a rise time (1 ps) similar to the X_0^{CS} bleaching and the SE rise time, and both the decay times (9 and 455 ps) comparable to the bleaching decay times τ_{d1} and τ_{d4} of the X_0^{CS} dynamics. This suggests that the 2.43 eV PA can be ascribed to PA from defect states close in energy to X_0^{CS}. On the contrary the 1.77 eV PA shows a very fast rise time (about of 300 fs) and a nonexponential decay with a fast relaxation (300 fs) followed by a slow decay similar to the 2.43 eV PA. Moreover the signal intensity is much lower than the 2.43 eV. These results suggest that 1.77 eV PA is partially due to PA from defects close to X_0^{CS} (as the 2.43 eV) and partially due to PA from defects states close to X_2, as observed in the core, which are not completely passivated by the shell and with low density (as suggested by the low signal). These states are quickly populated from X_2 after excitation and then rapidly relax to lower lying defect states in about 300 fs. Finally τ_{d1} and τ_{d4} bleaching time constants are assigned to relaxation from defect states to ground state.

The defects states close to X_0^{CS} involved in the PA processes, in the core/shell sample, can be ascribed to lattice strain relaxation, through the formation of extended defects at the core/shell interface, that cannot be ruled out in our samples, where a 0.80 ML thick shell has been overgrown, even if the graded CdS/ZnS shell used in this work is expected to reduce the lattice misfit between core and shell, compared to the usual ZnS shell. These defects can bring additional states in the midgap that act as traps and/or nonradiative recombination sites[12–14] competing with the development of gain. So the shell decreases the high density of surface states and avoids carriers trapping which occurs mainly from the higher excited state, as found in the core sample. However the shell introduces additional states in the midgap, which are involved in the photoabsorption processes. This process is schematized in the energy diagram shown in Fig. 12(b).

V. CONCLUSIONS

In this work we have studied the effect on relaxation processes of the surface and the interface, in core and core/shell quantum rods, respectively. In particular, in the core QRs we evidenced the role of the surface defects, whose energies result to be resonant to the highest QRs energy levels. These defects trap very efficiently the photoexcitated carriers and reduce the emission QY. In the core/shell sample this mechanism is suppressed by the passivation effect (due to the ZnS shell overgrowth around the CdSe core), and only intrinsic intraband relaxation processes are observed. However, despite the surface states passivation, which enhances the emission QY by one order of magnitude, the core/shell quantum rods exhibit a reduction of the SE, as compared to the core sample. Moreover, in the core/shell samples, net SE cannot be sustained for more than 25 ps due to a competing photoinduced absorption (PA) process, not present in the core sample. The photo-induced absorption processes are associated with carriers trapped at midgap states, which are likely to be introduced by the strain present in the shell. As a consequence we can deduce that also optical gain mechanism can be affected by the presence of the shell, because it is strongly dependent on SE and PA processes and we have observed that a thick shell modifies these mechanisms.

ACKNOWLEDGMENTS

We thank Professor P. Alivisatos (UC Berkeley) for the use of his laboratory facilities. Many thanks to Dr. D. Marinotto for valuable help with the pump and probe experiments. We take great pleasure in thanking Professor L. Vasanelli (Dip. di Ing. dell'Innovazione, Univ. di Lecce) and Professor R. Cingolani (NNL-INFM Lecce) for many useful discussions.

APPENDIX

The differential transmission signal at the emission wavelength of the sample ($\Delta T/T_{\mathrm{em}}$) is, in general, given by the superposition of absorbtion bleaching ($\Delta T/T_{\mathrm{em}}^{\mathrm{bl}}$), stimulated emission ($\Delta T/T_{\mathrm{em}}^{\mathrm{SE}}$), and photoinduced absorption ($\Delta T/T_{\mathrm{em}}^{\mathrm{PA}}$). In the limit of small signals, which is valid in the emission range of both samples, these signals are additive. In our analysis we determine the time interval in which

$$\frac{\Delta T/T_{\mathrm{em}}^{\mathrm{bl}} + \Delta T/T_{\mathrm{em}}^{\mathrm{SE}} + \Delta T/T_{\mathrm{em}}^{\mathrm{PA}}}{\Delta T/T_{X_0}^{\mathrm{bl}}} \geqslant \frac{\mathrm{Abs}_{\mathrm{em}}}{\mathrm{Abs}_{X_0}} = \frac{\Delta T/T_{\mathrm{em}}^{\mathrm{bl}}}{\Delta T/T_{X_0}^{\mathrm{bl}}}. \quad \text{(A1)}$$

The validity limit of the last identity has been already discussed in Ref. 31, from which it is evident to see that the imposed condition is equivalent to

$$\Delta T/T_{\mathrm{em}}^{\mathrm{SE}} + \Delta T/T_{\mathrm{em}}^{\mathrm{PA}} \geqslant 0 \Rightarrow |\Delta T/T_{\mathrm{em}}^{\mathrm{SE}}| \geqslant |\Delta T/T_{\mathrm{em}}^{\mathrm{PA}}|. \quad \text{(A2)}$$

*Also at ISUFI Institute for Advanced Interdisciplinary Studies, Universitá degli Studi di Lecce, Via per Arnesano, 73100 Lecce, Italy. Electronic address: arianna.creti@le.imm.cnr.it

[1] X. Peng, L. Manna, W. Yang, J. Wickham, E. Scher, A. Kadavanich, and A. P. Alivisatos, Nature (London) **404**, 59 (2000).
[2] L. Manna, E. C. Scher, and A. P. Alivisatos, J. Am. Chem. Soc. **122**, 12700 (2000).
[3] S.-H. Kan, T. Mokari, E. Rothenberg, and U. Banin, Nature (London) **2**, 155 (2003).
[4] W. U. Huynh, J. J. Dittmer, and A. P. Alivisatos, Science **295**, 2425 (2002).
[5] A. P. Alivisatos, Nat. Biotechnol. **22**, 47 (2004).
[6] J. Hu, L. Li, W. Yang, L. Manna, L. Wang, and A. P. Alivisatos, Science **292**, 2060 (2001).
[7] M. Kazes, D. Y. Lewis, Y. Ebenstein, T. Mokari, and U. Banin, Adv. Mater. (Weinheim, Ger.) **14**, 317 (2002).
[8] S. Link and M. El-Sayed, J. Appl. Phys. **92**, 6799 (2002).
[9] H. Htoon, J. A. Hollingworth, A. V. Malko, R. Dickerson, and V. I. Klimov, Appl. Phys. Lett. **82**, 4776 (2003).
[10] H. Htoon, J. A. Hollingsworth, R. Dickerson, and V. I. Klimov, Phys. Rev. Lett. **91**, 227401 (2003).
[11] L. Manna, E. C. Scher, L.-Shi Li, and P. Alivisatos, J. Am. Chem. Soc. **124**, 7137 (2002).
[12] T. Mokari and U. Banin, Chem. Mater. **15**, 3955 (2003).
[13] X. Peng, M. C. Schlamp, A. V. Kadavanich, and A. P. Alivisatos, J. Am. Chem. Soc. **119**, 7019 (1997).
[14] B. O. Dabbousi, J. Redriguez-Vejo, F. V. Mikulec, J. R. Heine, H. Mattousi, R. Ober, K. F. Jensen, and M. G. Bawendi, J. Phys. Chem. B **101**, 9463 (1997).
[15] Y. W. Cao and U. Banin, J. Am. Chem. Soc. **122**, 9692 (2000).
[16] M. Lomascolo, A. Cretí, G. Leo, L. Manna, and L. Vasanelli, Appl. Phys. Lett. **82**, 418 (2003).
[17] C. Ricolleau, L. Audinet, M. Gandais, and T. Gacoin, Thin Solid Films **336**, 213 (1998).
[18] T. S. Li and K. J. Kuhn, J. Comput. Phys. **110**, 292 (1994).
[19] M. Sadkane and R. B. Sidje, Numer. Algorithms **20**, 217 (1999).
[20] C. W. Murray, S. C. Racine, and E. R. Davidson, J. Comput. Phys. **103**, 382 (1992).
[21] U. E. H. Laheld and G. T. Einevoll, Phys. Rev. B **55**, 5184 (1997).
[22] D. Katz, T. Wizansky, O. Millo, E. Rothenberg, T. Mokari, and U. Banin, Phys. Rev. Lett. **89**, 086801 (2002).
[23] M. E. Schmidt, S. A. Blanton, M. A. Hines, and P. Guyot-Sionnest, Phys. Rev. B **53**, 12629 (1996).
[24] J. Li and J.-B. Xia, Phys. Rev. B **61**, 15880 (2000).
[25] L. M. Ramaniah and S. V. Nair, Phys. Rev. B **47**, 7132 (1993).
[26] Al. L. Efros, M. Rosen, M. Kuno, M. Nirmal, D. J. Norris, and M. Bawendi, Phys. Rev. B **54**, 4843 (1996).
[27] V. I. Klimov, J. Phys. Chem. B **104**, 6112 (2000).
[28] V. Klimov, S. Hunsche, and H. Kurz, Phys. Rev. B **50**, R8110 (1994).
[29] V. I. Klimov, D. W. McBranch, C. A. Leatherdale, and M. G. Bawendi, Phys. Rev. B **60**, 13740 (1999).
[30] V. I. Klimov and M. G. Bawendi, MRS Bull. **26**, 998 (2001).
[31] In our measurements the $\Delta T/T_{X_0}^{\mathrm{bl}}$ is 43% (15%) for the core/shell (core) sample. The approximation of this signal, which is not rigorously small, with $-\Delta\alpha d$ leads to overestimate $\Delta T/T_{\mathrm{em}}^{\mathrm{bl}}$ of about 20% (8%) of its value for the core/shell (core). $\Delta T/T_{\mathrm{em}}^{\mathrm{bl}}$ should be then even smaller that the estimated one, which is anyway already much smaller than the positive signal observed in the emission region of both samples.
[32] A. V. Malko, A. A. Mikhailovsky, M. A. Petruska, J. A. Hollingsworth, and V. I. Klimov, J. Phys. Chem. B **108**, 5250 (2004).
[33] X. Ai, R. Jin, Ch. Ge, J. Wang, Y. Zou, X. Zhou, and X. Xiao, J. Chem. Phys. **106**, 3387 (1997).
[34] P. T. Landsberg, *Recombination in Semiconductors* (Cambridge University Press, Cambridge, England, 2003), Chap. 5.3.